On the Finite Element Discretization of Continuous Tow-Sheared Structures

Calum J. McInnes*, Reece L. Lincoln†, Alberto Pirrera‡, Byung Chul Kim§, and Rainer M. J. Groh¶
Bristol Composites Institute, University of Bristol, Queen's Building, University Walk, Bristol, BS1 8TR, UK

Tow-steered laminates, those in which the fiber angle varies as a function of in-plane coordinates, represent a substantial numerical modeling problem. In the Continuous Tow Shearing (CTS) process, the tows are deformed by in-plane shearing that generates a non-linear orientation-thickness coupling, which needs to be accounted for when analyzing CTS structures. In this manuscript, an investigation into the Finite Element discretization of CTS structures is conducted to ascertain the most appropriate element choice in terms of computational cost and accuracy. First, natural frequency and buckling eigenvalue analyses are conducted on constant-thickness flat plates and thin-walled cylinders ($[\pm 45/0/90]_s$ layup), in order to set a baseline. Next, multiple discretization strategies are implemented to investigate a CTS plate and a thin-walled CTS cylinder by means of two- and three-dimensional shell elements, in linear frequency and buckling analyses. Two CTS stacking sequences are considered, with the first ($[\pm 0\langle 0|70\rangle^{10}]_{2s}$) having identical steering across plies, and the second with variable steering across plies ($[\pm 0\langle 0|70\rangle^{10}/\pm 90\langle 0|70\rangle^{10}]_s$) to increase the discretization difficulty. The use of three-dimensional shell elements allows for greater fidelity in representing the geometry of a CTS structure, as they allow the asymmetric thickness build-ups to be discretized accurately. We show that three-dimensional shell elements enable the use of lower mesh resolutions whilst maintaining solution accuracy, in comparison to two-dimensional shell element meshes of the same geometric in-plane resolution. Moreover, a relation between element type and mesh resolution is presented to appropriately align element centroids and nodal coordinates, for two- and three-dimensional shell elements, respectively, with the maxima of a specific thickness distribution.

I. Nomenclature

A_i	=	Planar area of i^{th} mesh iteration
L	=	Plate and cylinder longitudinal dimension
l	=	Length of single shearing period
N	=	Number of plies in laminate
n	=	Shearing periodicity
n^{e}	=	Number of elements in mesh
n_i^{e}	=	Number of elements comprising i^{th} mesh iteration
R	=	Cylinder radius
T_0	=	Starting fiber reference path angle, taken clockwise from ϕ
T_1	=	Ending fiber reference path angle, taken clockwise from ϕ
t_0, t	=	Tow thickness of a ply pre- and post-shearing, respectively
t_i	=	Thickness of i^{th} mesh iteration
t_{lam}	=	Laminate total thickness
W	=	Plate transverse dimension
θ	=	Local fiber angle taken from global x-axis
ϑ	=	Angle made with horizontal axis of a trigonometric circle

*PhD Student, Bristol Composites Institute, University of Bristol, UK
†PhD Student, Bristol Composites Institute, University of Bristol, UK
‡Associate Professor of Nonlinear Structural Mechanics, Bristol Composites Institute, University of Bristol, UK
§Associate Professor in Composites Design and Manufacture, Bristol Composites Institute, University of Bristol, UK
¶Lecturer in Digital Engineering of Structures, Bristol Composites Institute, University of Bristol, UK

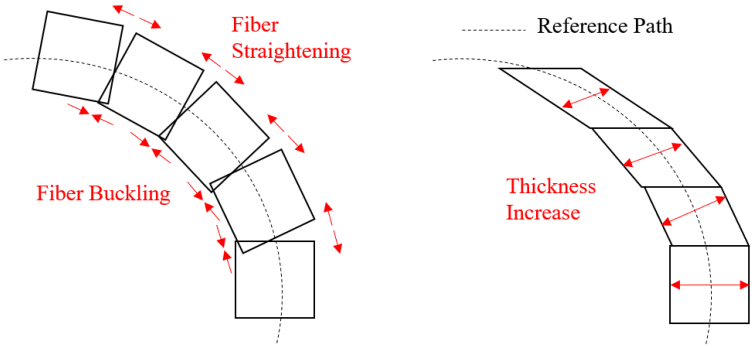

(a) Tow Steering by AFP **(b) Tow Steering by CTS**

Fig. 1 Tow deformation mechanisms to achieve tow steering along a reference path by in-plane bending using AFP (a) in-plane shearing using CTS (b). Reproduced from Ref. [7].

$\lambda_i^{\text{fr}}, \lambda_f^{\text{fr}}$ = Frequency eigenvalue of the i^{th} and final mesh iteration
$\lambda_i^{\text{Pcr}}, \lambda_f^{\text{Pcr}}$ = Buckling eigenvalue of the i^{th} and final mesh iteration
ϕ = Angle from global x-axis of part which denotes unsheared direction

II. Introduction

In aerospace structural applications, composite materials are widely adopted due to their desirable properties, such as high specific stiffness and strength. Such properties allow for increased payload fractions and improved fuel efficiency for both air and space vehicles. Commonly employed composite design philosophies rely on fibers within each ply of a laminate being straight and aligned along load paths to meet set design criteria, such as stiffness and strength [1]. The inherent material anisotropy of composites allows for the potential of local tailoring with improved alignment between fiber orientation and load path [2]. Stiffness variations can be introduced in a laminated structure by a number of methods, such as overlapped patches and ply drop-offs [2]. Most novel is the concept of Variable Angle Tow (VAT) composite structures, where the fiber angle varies with position in a ply [3].

The most commonly investigated method of manufacturing VAT composites is the Automated Fiber Placement (AFP) process [4]. AFP has typically been the process of choice due to its ease of adoption in industrial settings and its ability to deposit material onto curved tool surfaces [5]. However, AFP-manufactured VAT structures are prone to process-induced defects, such as fiber wrinkling and resin rich areas [6]. The presence of defects is due to the fundamental material deformation mechanism when steering material tows by AFP—the steering being achieved through in-plane bending of the tows along a curvilinear reference path [7]. This in-plane bending mechanism of the material causes buckling on the inner and straightening on the outer radii of the material tow [7], as shown in Figure 1. Both buckling and straightening of the material tow result directly in wrinkles and resin rich areas which can reduce structural performance [6]. Furthermore, these defects represent a significant complication to modeling. Indeed, while buckling and straightening can be limited or even eliminated by controlling a tow's steering radius, by bending material tows when steering by AFP, a fiber reference path cannot be tessellated and thus tow gaps or overlaps must be created to complete a single ply. Therefore, the presence of gaps and overlaps cannot be avoided and, in addition to wrinkles and resin rich areas, further compounds to reduce strength and increase modeling difficulty, especially in the discretization of geometries for definition of a Finite Element (FE) mesh [8]. Moreover, prediction of the location of such manufacturing features and defects is not trivial. For modeling such structures, Fayazbakhsh *et al.* proposed a "defect layer method" to reduce the stiffness of elements that represented regions of tow gaps or overlaps by increasing the element thickness [9].

When modeling perfect AFP tow-steered structures, Labans *et al.* utilized a simple discretization methodology to model VAT cylinders buckling under axial compression. A number of perpendicular partitions along the longitudinal axis of the cylinder were introduced to the two-dimensional shell elements, henceforth referred to as conventional shell elements', mesh to assign regions of constant layup [10]. This method did not account for any manufacturing induced defects in the AFP modeling strategy but showed reasonable correlation to experimental results. Similarly, Rouhi *et al.* [11] assigned a number of constant fiber angle bands around the circumference of a VAT cylinder under

bending-induced buckling. Rouhi *et al.* [11] employed 8-node conventional shell elements. However, due to the lack of thickness variations, 4-node shell elements would have been equally valid for modeling. Generally, the method by Labans *et al.* [10] is only valid for tow-steering along the cylinder's longitudinal axis, whereas the method by Rouhi *et al.* [11] is valid for tow steering around the circumference. Additionally both Labans *et al.* [10] and Rouhi *et al.* [11] employed conventional shell elements in their investigations. Labans *et al.* [10] used a simple 4-node shell and Rouhi *et al.* [11] used an 8-node shell. Rouhi *et al.* [11]'s use of 8-node shell elements posses the ability for additional degrees of freedom to be defined at an internal mid-body node [12]. The reasoning for the use of 8-node shells by Rouhi *et al.* [11] was not commented on, however the additional nodes may allow for greater discretization of the in-plane stiffness variations of tow-steered structures. Overall, from a modeling perspective, these methods produce a numerically coarse description of the spatial variation in fiber orientation, allowing for all plies of a tow-steered laminate to be steered in one direction only, and do not consider process-induced defects. Subsequently, Tatting *et al.* found element-wise assignment of fiber angles to be most appropriate for modeling VAT cylinders [13]. When compared directly to Labans' and Rouhi's methods, Tatting's method assigned constant layups per element on a tow-steered mesh, which allowed for a far greater level of control over the geometric discretization of a tow-steered structure.

As the structural performance of VAT structures by AFP manufacture suffers under presence of process-induced defects, a new process for tow steering, Continuous Tow Shearing (CTS), was developed by Kim *et al.* [7]. CTS employs a fundamentally different material deformation mechanism to manufacture tow-steered structures than the AFP process. Instead of bending material tows, the CTS process shears them in-plane [7], see Figure 1. Due to the mechanics of material shearing, no defects, such as those seen in AFP manufactured structures, are caused by CTS. The in-plane shearing of material tows allows for VAT laminates to be manufactured without gaps or overlaps due to the perfect tessellation of a reference path across a ply. Of additional benefit, perfect tessellation allows for comparatively simpler structural modeling methodologies to be used when seeking to accurately identify material distribution in a CTS structure for subsequent discretization [7].

A mechanical consequence of the in-plane shearing of material tows by the CTS process is the change of their thickness. Geometrically, this material thickness change is related to the shearing angle imposed by the CTS process, where the shearing angle is simply the difference between the steering direction, controlled by ϕ, and the local fiber angle, θ. The increase in thickness of a ply of a CTS structure can be calculated by simply assuming volume conservation of a tow pre- and post-shearing, with Eq. (1) denoting the thickness increase [7]:

$$t = t_0 \cdot \sec(\theta - \phi). \tag{1}$$

where, t and t_0 are the thickness of the ply post- and pre-shearing, respectively. The maximum shearing angle achievable by the CTS process is $\theta - \phi = 70°$, as demonstrated by Kim *et al.* [14]. The relation between positional fiber angle and thickness across a non-dimensionalized half shearing period is visualized upon inspection of Figure 2, where, dependent upon the magnitude of shearing, a consequential thickness increase arises.

It is of note that this orientation-thickness coupling is not to the detriment of structural performance, such as the process-induced defects present in AFP manufactured tow-steered structures. As Kim noted, the thickness buildup could be exploited to provide enhanced stiffness over a straight tow comparison [7]. This potential for increased structural performance by embedding stiffening features into a laminate was investigated by Lincoln *et al.*, who studied embedded longitudinal stringers and circumferential hoops on a thin-walled cylinder to decrease structural sensitivity to geometric imperfections under axial compression [15]. Subsequently, Lincoln *et al.* utilized a genetic algorithm to optimize cylinders to identify the potential for structural imperfection insensitivity [16].

Tow-steered structures have thus been the subject of numerous FE studies, however little formal investigation into the most accurate element choice for FE modeling of CTS tow-steered structures exists, due to a widespread continuation of choices taken from AFP studies. When FE modeling CTS structures, authors such as Lincoln *et al.* [15, 16], Kim *et al.* [17], Groh and Weaver [18], use degenerated shell elements. This manuscript shall refer to these degenerated shell elements as 'conventional shell elements' (S4 or S4R in Abaqus CAE). It is believed that the reason for this element choice in modeling is twofold. Firstly, it allows for the most straightforward discretization of a tow-steered reference path; and, secondly, it is a continuation of the S4R element choice when modeling AFP tow-steered structures, such as that employed by White *et al.* [19]. For FE modeling tow-steered structures with no thickness variation, i.e. those manufactured by AFP, a conventional 4-node element choice is sufficient to capture the variation in fiber angle across a ply. However, this manuscript investigates the need for accurate geometrical representation of the out-of-plane thickness variation of CTS tow-steered laminates by utilizing three-dimensional shell elements, referred to as 'continuum shell elements' in Abaqus CAE, for increased accuracy in geometric approximation.

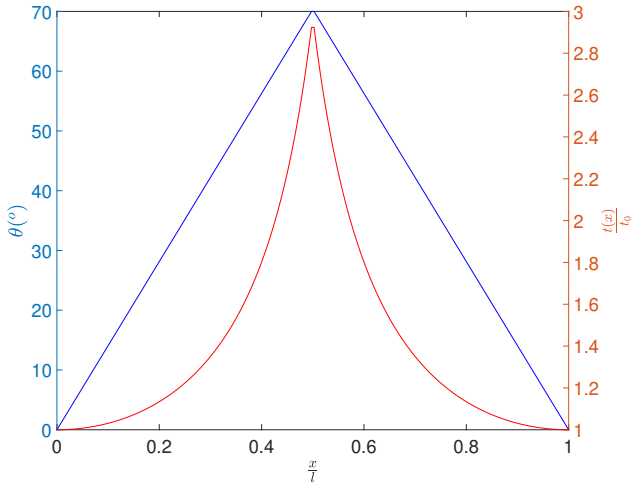

Fig. 2 Mechanical coupling of fiber orientation and thickness pre- and post-shearing for an arbitrary $\langle T_0|T_1\rangle$ tow-steered ply of linear angle variation by CTS. Note maximum shearing angle of 70° corresponds to a $3\times$ increase in thickness. Furthermore, this inherent mechanical coupling is non-linear.

This manuscript is structured as follows. Subsection II.A outlines the notation required for tow steering of a composite ply by CTS. Section III outlines a methodology for formulating FE models of CTS structures. The method is subsequently implemented in Abaqus CAE for two common structural elements: a flat plate and a thin-walled cylinder under two load cases: frequency and compression buckling. Section V presents numerical results into the use of continuum over convectional shell elements when modeling CTS structures. Firstly, a consideration of element type for modeling constant-angle, constant-thickness structures is presented to contextualize the later work. This work is an investigation into the potential for solution performance benefit when meshing CTS structures with three-dimensional, henceforth referred to as 'continuum' shell, over the commonly used conventional shell elements. As CTS structures are both variable angle and variable thickness, the additional node definition of continuum shell elements is identified as a potential modeling choice that better discretizes the thickness variations present in CTS structures. This improved discretization allows for coarser continuum than conventional shell element meshes to be used in analyses. The use of coarser meshes gives benefits to design studies which involve large computational runs. Finally, Section VI summarizes the key findings of the manuscript and makes closing recommendations for modeling strategies for CTS structures.

A. CTS Ply Definition

The design of a VAT laminate by CTS requires a notation for the consistent definition of fiber path variation within a ply. This manuscript employs a linear fiber angle variation, which is the lowest-order variation one can employ and is defined by

$$\theta(x) = \begin{cases} \phi + \frac{T_1 - T_0}{l/2} x + T_0, & \text{if } 0 \le x \le \frac{l}{2} \\ \phi + \frac{T_0 - T_1}{l/2}(x - \frac{l}{2}) + T_1, & \text{if } \frac{l}{2} < x \le l \end{cases} \tag{2}$$

where ϕ represents the angle from the global x-axis, and T_0 and T_1 represent clockwise angles from ϕ at two locations of the domain with linear fiber angle variation in between. The shearing period over coordinate x in the direction of ϕ occurs over period length l. The period length is directly controlled by the steering direction, where if $\phi = 0^\circ$, l is equal to the global x-direction dimension of the structure. Similarly if $\phi = 90^\circ$, l is equal to the global y-direction dimension.

Moreover, due to the aforementioned orientation-thickness coupling of material tows when tow steering by CTS, a consideration of thickness variation must be made. The thickness of a material tow steered by the CTS process is denoted previously in Eq. (1). The notation used throughout this manuscript is extended from that initially proposed by Gürdal *et al.* [20] and adapted for use in CTS structures by Lincoln *et al.* [15], where a single steered ply with linear variation in fiber angle is denoted by

$$\phi\langle T_0|T_1\rangle^n \tag{3}$$

where periodicity is introduced to repeat a single fiber angle variation, $T_0 \rightarrow T_1 \rightarrow T_0$, in the steering direction, ϕ. This periodicity is denoted by n, where the maximum potential periodicity is controlled by the minimum steering radius

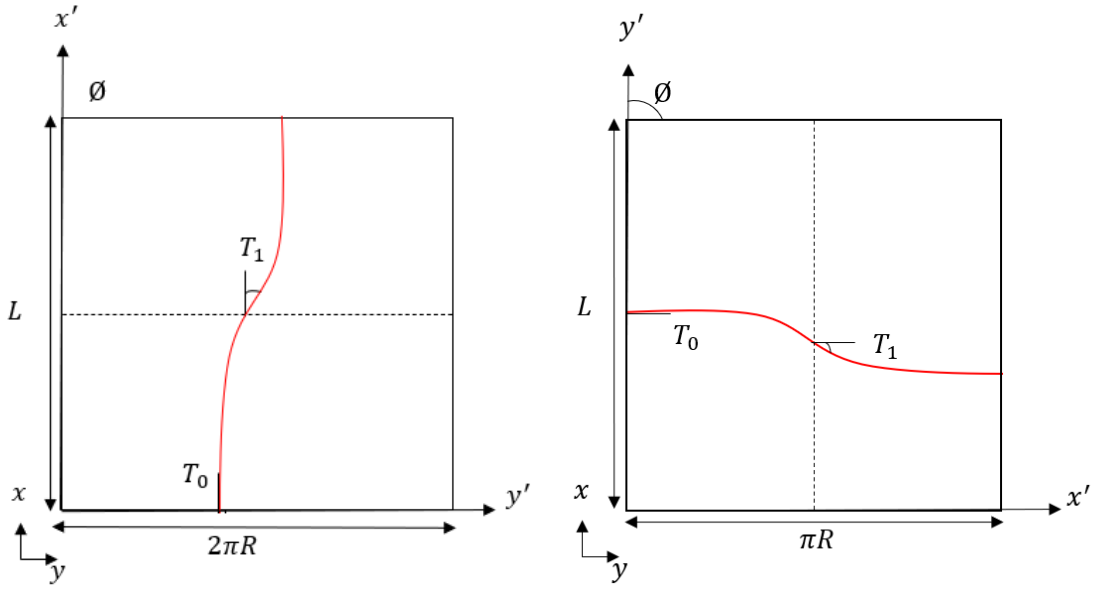

(a) $\phi = 0°$, $n = 1$ **(b)** $\phi = 90°$, $n = 2$

Fig. 3 Periodic steering of a unit cell upon a thin-walled cylinder, visualized for the two steering directions considered; (a) $\phi = 0°$ and (b) $\phi = 90°$. Note if $T_1 > T_0$ the thickness build-ups will occur at the middle of the shearing period.

of the CTS process [14] and the steering direction. In this manuscript a $\phi = 0°$ steering direction denotes steering along the part x-axis. This notation is visualized in Figure 3, whereby a cylindrical tow-steered path has been unrolled and the directional periodic variation in fiber angle between T_0 and T_1 across a ply is visualized for the two steering directions chosen in this manuscript, $\phi = 0°$ and $\phi = 90°$. The number of thickness build-ups in a ply is controlled by the periodicity of the fiber path.

III. Model

Modeling methodologies are developed for discretizing by two-dimensional conventional shell (S4R in Abaqus CAE) or three-dimensional continuum (SC8R in Abaqus CAE). A script is implemented in MATLAB R2021b [21] to produce Abaqus 2018 [12] input files which are submitted to the numerical solver. The primary difference in usage of these elements is in the through-thickness node definition in the element assignment. Conventional shell elements only require node definition at the reference surface of a three-dimensional body. Comparatively, continuum shell elements require node definition for the full three-dimensional body.

Firstly, the geometry of a structure (a flat plate and thin-walled cylinder are considered in this manuscript) is defined by numerical discretization to generate nodes for construction of the FE mesh. Conventional shell element nodal coordinates for a flat plate are required only in the x-y plane. Whereas for a cylinder, nodes are given (x, y, z) coordinates, in which the cylinder coordinates are found as

$$(x_1, y_1, z_1) = (x, R\cos\vartheta, R\sin\vartheta) \tag{4}$$

to give a cylinder of radius R. 4-node conventional shell elements (S4R) are formulated by a meshing algorithm which assigns elements through a counterclockwise numbering convention [12]. Comparatively, 8-node continuum shell elements (SC8R) formulation requires an additional layer of nodal coordinates for element definition, where the additional layer of nodes, for a cylinder is computed as simply

$$(x_2, y_2, z_2) = (x, (R + t_{\text{lam}})\cos\vartheta, (R + t_{\text{lam}})\sin\vartheta) \tag{5}$$

where t_{lam} is the total thickness of the laminate, geometrically defined as $N \times t$, here N is the number of plies in the laminate.

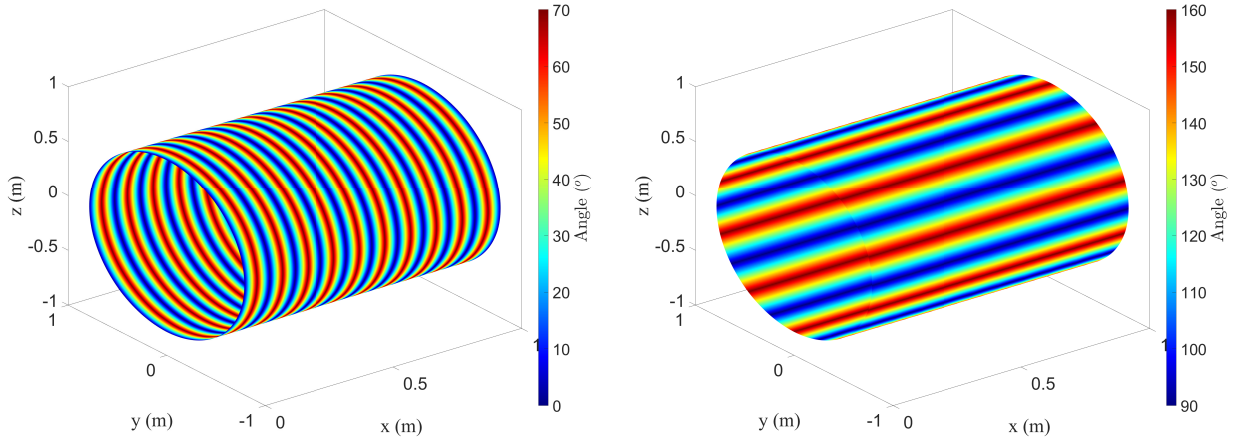

(a) Axial Tow Steering by CTS **(b) Circumferential Tow Steering by CTS**

Fig. 4 Steering of angles to give fiber angle distributions in the axial direction by (a) $\phi = 0°$ and circumferential by (b) $\phi = 90°$ on a thin-walled cylinder of dimensions $L = R = 1$ m. Note the periodicity of the resulting pattern in spatial angle variation and hence ability to extract constant-angle 'slices'. Note, all angles are taken with respect to the x-axis, following the convention of Lincoln [15]

To model CTS structures, which are both variable-angle and variable-thickness, the notation presented in Section II.A is implemented by inferring that constant fiber angle 'slices' may be taken of the structure upon discretization due to the perfect tesselation of material tows by the CTS process. For example, consider Fig. 4a, where the material tows are being steered along the cylinder's longitudinal axis. A constant fiber angle can be extracted around the circumference due to tessellation. Similarly, for circumferential steering in Fig. 4b, constant fiber angle 'slices' can be assigned. The geometry of these constant-angle 'slices' is formulated by consideration of both the structural geometry and CTS layup design. This notion of constant fiber angle 'slices' is similar to that of the partitioning method used by Labans *et al.* [10]. However, this method employs a far finer discretization, such that each element within a mesh is assigned unique properties depending upon the chosen CTS layup design and the element's position . To further aid computational efficiency in model formulation, a ply-level unit cell can be defined. From Fig. 4, it is clear that the logical choice of a unit cell for a ply is a single shearing period, i.e. a single $T_0 \rightarrow T_1 \rightarrow T_0$ variation. The formulation of a unit is visualized in Fig. 3 for a thin-walled cylinder. Additional modeling efficiency can be introduced if considering laminates which follow conventional design rules, such as being balanced and/or symmetric. A balanced or symmetric laminate reduces the number of unique spatial variation computations by a factor of 2. If combined a balanced and symmetric laminate reduces the unique computations by a factor of 4.

The element type chosen for structural modeling dictates whether fiber angles must be computed at element centroids only or also at nodal locations. A current limitation of the commercial FE software employed in this work, Abaqus 2018, is that only a single fiber angle can be assigned per ply within a section. There is potential within Abaqus CAE to assign stiffness matrices at integration points by means of full integration shell elements and user subroutines [12]. However, this will incur additional computational cost in the software pre-processor as multi-thread operation is currently not supported, unlike in the solver [12]. Thus, for the reduced integration elements chosen within this work the calculation of fiber angles at nodes is for continuum shell element geometry definition not section assignment. Irrespective of element type chosen, the fiber angle must be computed at the element centroids for section assignment.

In addition to computation of fiber angles at nodes and element centroids, the corresponding thickness variations must be also represented due to the orientation-thickness coupling of tow steering by CTS. For thickness computation, through-thickness dummy nodes and centroids are utilized to represent the required offsets due to a thickness variation. The positional thickness is found by simple summation of these dummy nodes as Eq. (6) and 7, and as such can reflect the potential for layup offset in either the positive or negative z-direction.

$$t(x, W) = \sum_{k=1}^{N} t_0^k \cdot \sec((\theta^k(x, W) - \phi^k) \tag{6}$$

Table 1 Material properties of MTM-43/T800, reproduced from [16]

E_1 (GPa)	E_2 (GPa)	G_{12} (GPa)	G_{13} (GPa)	ν_{12}	G_{23} (GPa)	ρ (kg/m^3)	t_0 (mm)
122	7.32	4.9	4.9	0.31	3.23	1590	0.13

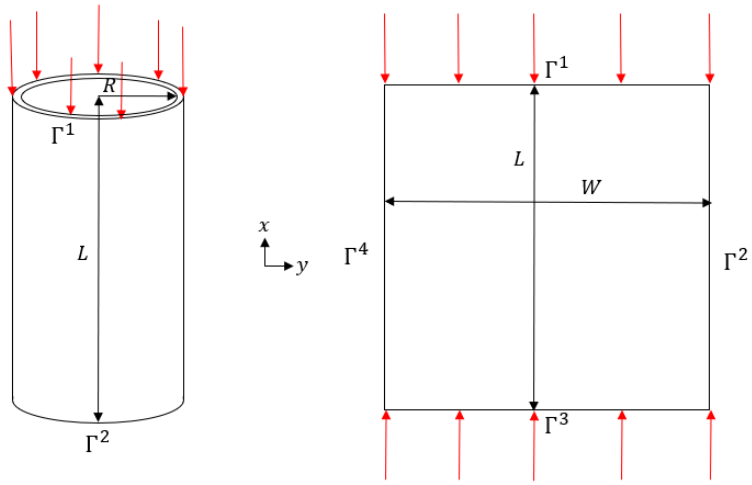

Fig. 5 Load introduction for critical buckling load computation of thin-walled cylinder and flat plate. Arrows show direction of load with respect to global coordinate system. Note orientation of global coordinate system.

$$t(L, y) = \sum_{k=1}^{N} t_0^k \cdot \sec((\theta^k(L, y) - \phi^k) \tag{7}$$

IV. Problem Definition

Both a unit tow-steered CTS flat plate and thin-walled cylinder ($L_{\text{plate}} = W_{\text{plate}} = L_{\text{cylinder}} = R_{\text{cylinder}} = 1$ m) are fully geometrically discretized by the prior methodologies to investigate the potential benefit of additional node definition by use of continuum shell elements. These two structures are chosen due to wide applicability to aerospace design scenarios and, more pertinently, the increase in geometrical curvature. The carbon-epoxy material system used in this manuscript is MTM-43/T800, with orthotropic properties presented in Table 1.

All structures in this manuscript are laminates where the bottom-most ply is stacked onto a tool surface such that the element normal is directed outwards. Furthermore, the structures are subjected to a linear eigenvalue approximation of both natural frequency and critical buckling load; two common aerospace design drivers.

When computing fundamental frequency each structure has no constraints on any edge, hence edges Γ^1 and Γ^2 (see Fig. 5) on the thin-walled cylinder are free; similarly, edges Γ^1, Γ^2, Γ^3 and Γ^4 on the flat plate are free. For each structure an eigenvalue prediction of resonant frequency is conducted in Abaqus Standard. Comparatively, when computing critical buckling loads of each structure constraints must be enforced. The buckling setup of both structures follows two classical structural mechanics problems. Namely, axial compression buckling of a thin-walled cylinder and compression buckling of a simply supported plate. Thus, to numerically represent these problems boundary conditions are introduced to allow only vertical translation on edge Γ^1 of the thin-walled cylinder, with edge Γ^2 is fully fixed. All edges of the flat plate are free to translate and rotate in-plane but not out-of-plane. The general buckling problem setup is visualized in Fig. 5, where the edges Γ^1, Γ^2, Γ^3 and Γ^4 are identified and the loading conditions are specified. Models are formulated with both conventional and continuum shell elements. Both conventional and continuum shell elements have equal degrees of freedom (DOF), where conventional shells posses 3 translational and 3 rotational DOFs per node. Comparatively continuum shell elements have 3 translational DOFs per node. Constant-thickness meshes are iteratively increased in resolution from 10×10 to 200×200 in increments of 10×10 to study the effects of element choice on eigenvalue convergence for both linear frequency and buckling analysis. Comparatively, the variable thickness nature

Table 2 CTS Layups Considered. Resulting thickness build-ups are presented in Fig. 6.

Number	Layup
1	$[\pm 0\langle 0\vert 70\rangle^{10}]_{2s}$
2	$[\pm 0\langle 0\vert 70\rangle^{10}/\pm 90\langle 0\vert 70\rangle^{10}]_{s}$

Table 3 Meshes required for 1% convergence for constant-thickness structures. N.B. run time refers to solver CPU time and converged mesh refers to a mesh of n^2 elements.

Structure	Analysis	Element Type	Converged Mesh	Run Time (s)
Plate	Frequency	S4R	20	1
		SC8R	20	2
Plate	Buckling	S4R	50	1
		SC8R	70	1
Cylinder	Frequency	S4R	50	3
		SC8R	30	3
Cylinder	Buckling	S4R	100	139
		SC8R	110	313

of CTS structures is expected to require finer meshes than that for constant-thickness structures, hence meshes are iteratively increased in resolution from 50×50 to 600×600 in increments of 25×25.

The objective of this manuscript is to consider whether the use of continuum shell elements represents a worthwhile modeling consideration when studying CTS structures. As CTS structures are variable angle, and more pertinently, variable thickness, it is expected that there is potential for the use of coarser meshes when using continuum shell elements. It is hypothesized that coarser continuum than conventional shell meshes may be employed due to the ability of continuum shell elements to more accurately discretize the thickness variations of CTS structures. By accurate capture of the thickness variations, comparatively fewer elements may be used and thus a reduction in computational solution time is expected.

V. Results

Firstly, in subsection V.A, an investigation into the use of conventional and continuum shell elements is considered for constant-angle, constant-thickness structures. These constant-angle, constant-thickness structures represent a simple discretization problem of 'standard' laminated structures. Next, in subsection V.B, a comparison of two CTS tow-steered structures (flat plate and thin-walled cylinder) is made to identify the need for modeling with elements that allow for full geometrical discretization. For each structure type, two CTS stacking layup designs of increasing discretization difficulty are investigated. Hence, each model is discretized by conventional and continuum shell elements, and accuracy is subsequently compared to a mesh of fine resolution. In this manuscript convergence is defined when

$$|1 - (\lambda_i/\lambda_f)| \leq 0.01, \tag{8}$$

where λ_i and λ_f are the resulting eigenvalues of the current (i) and the final (f) mesh iteration. The effects of increasing mesh resolution, defined by number of elements per unit area, i.e. n_i^{e}/A_i, where n_i^{e} and A_i are the number of elements and planar area of the i^{th} mesh iteration are investigated.

A. Constant-Thickness Structural Discretization By Shell Elements

In the analysis of constant-thickness, constant-angle plate with layup $[\pm 45/0/90]_{\mathrm{s}}$, the choice between continuum and conventional shell element shows no difference when undertaking a linear eigenvalue frequency analysis. The effects of increasing mesh resolution upon solution accuracy is presented in Fig. 7.

As presented in Fig. 7, there exists few cases where the use of conventional over continuum shell elements, or vice-versa, represents a significant avenue for increased computational solution efficiency. As is evident, the outlier in

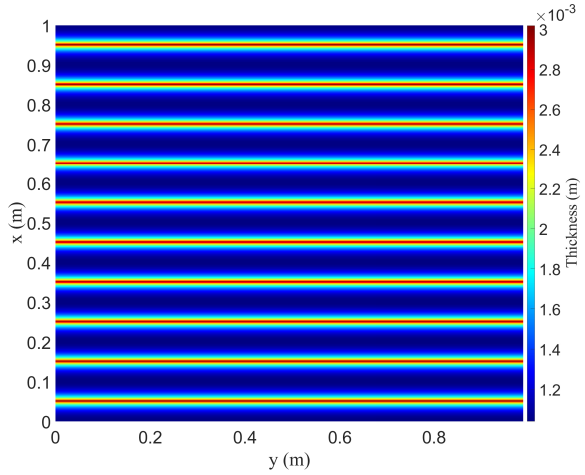

(a) Layup 1 ($[\pm 0\langle 0|70\rangle^{10}]_{2s}$) **Flat Plate**

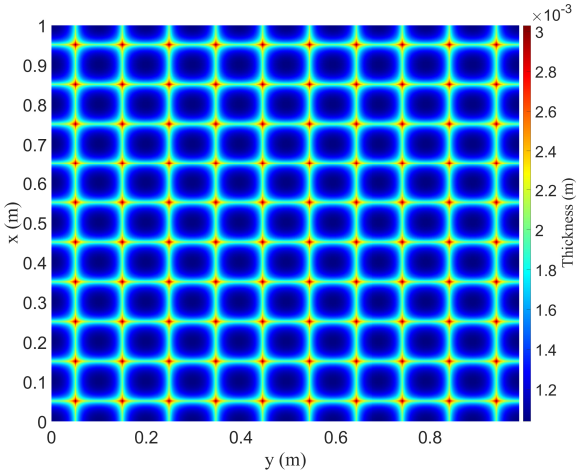

(b) Layup 2 ($[\pm 0\langle 0|70\rangle^{10}/\pm 90\langle 0|70\rangle^{10}]_{s}$) **Flat Plate**

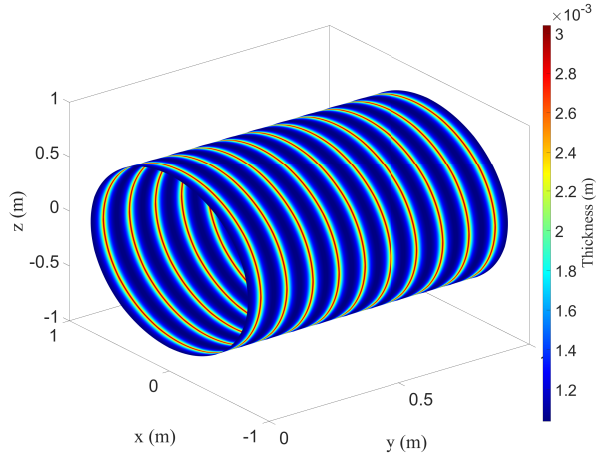

(c) Layup 1 ($[\pm 0\langle 0|70\rangle^{10}]_{2s}$) **Thin-Walled Cylinder**

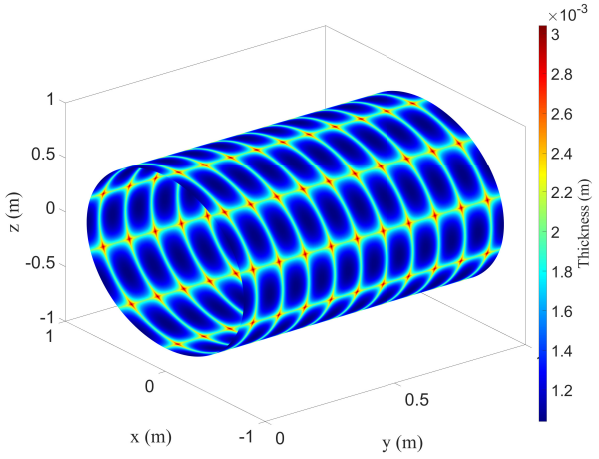

(d) Layup 2 ($[\pm 0\langle 0|70\rangle^{10}/\pm 90\langle 0|70\rangle^{10}]_{s}$) **Thin-Walled Cylinder**

Fig. 6 Thickness build ups resulting from Layups 1 **and** 2 **presented on the flat plate and thin-walled cylinder. Meshes are** 400×400 **for the flat plates in (a) and (b). The thin-walled cylinders, presented in (c) and (d) need comparatively finer meshes for accurate thickness build-up representation due to the larger unrolled dimensions, i.e.** $L_{\text{plate}} = W_{\text{plate}} = L_{\text{cylinder}} = R_{\text{cylinder}} = 1$ **m, thus** $A_{\text{plate}} = L \times W$ **and** $A_{\text{cylinder}} = L \times 2\pi R$**, and hence are represented by** 600×600 **meshes. All figures denote thickness computations at nodal locations by use of continuum shell elements. Note Layup** 1 **corresponds to thickness build-ups aligned in the global** y**-direction due to steering in the** x**-direction. Additionally, the mixed steering of Layup** 2 **renders thickness build-ups aligned in both the global** x**- and** y**- directions. Regardless of steering directions the magnitude of the thickness build-ups is constant.**

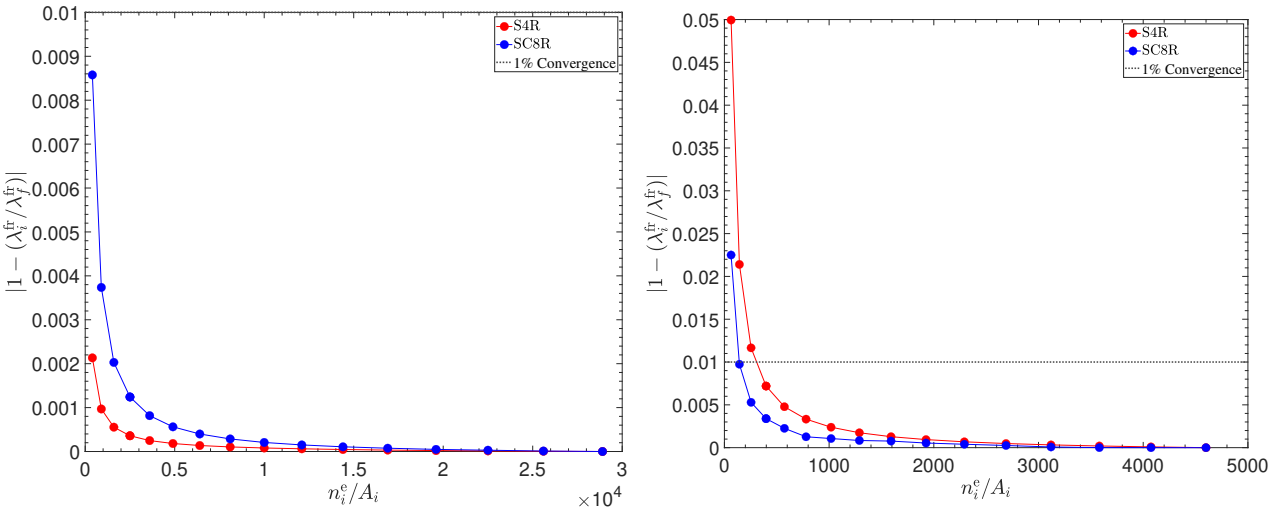

(a) Constant-thickness Plate Frequency

(b) Constant-thickness Cylinder Frequency

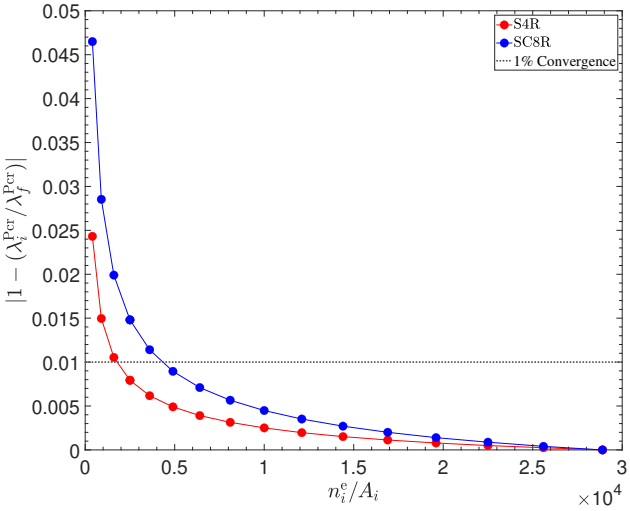

(c) Constant-thickness Plate Buckling

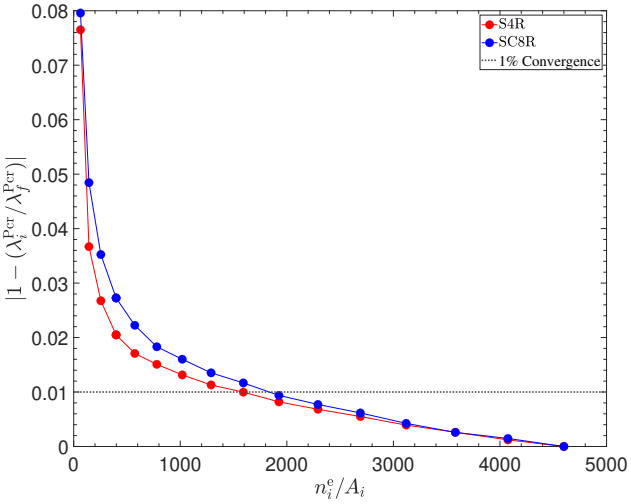

(d) Constant-thickness Cylinder Buckling

Fig. 7 Constant-thickness structure eigenvalue approximation of frequency and buckling eigenvalues for each considered structure (flat plate and thin-walled cylinder). Mesh resolutions required for 1% convergence of resulting linear frequency and buckling eigenvalues are presented in Table 3.

the data is the cylinder buckling analyses, presented in Fig. 7d. Cylinder buckling, in comparison to the other analyses is the most difficult to approximate and as such, both the mesh resolutions and run time requirements are substantially greater. When comparing the constant-thickness cylinder, Fig. 7d to the other three figures, Figs. 7a, 7c and 7b, it is clear that the rate of convergence for both element types is slower than that presented for the others. Moreover, the continuum shell element mesh required for 1% convergence is only 21% finer, yet the run time requirement is 125% greater. Thus, the relation between mesh resolution and run time is highly non-linear, whereby a single iteration later requires a substantially higher solver time. It is expected that the curvature of the constant-thickness cylinder compounded with complex mode shapes arising during buckling contributes to this increased required meshing resolution and resulting run times.

Both the constant-thickness plate frequency and buckling analyses presented in Figs. 7a and 7c show similar behavior. The constant-thickness plate frequency analyses shows no benefit to either element types, both element types achieve 1% convergence at the same mesh resolutions. The plate, implicitly, is flat and the mode shapes arising are simple, hence coarse meshes can be used. The meshes required are only fine enough to capture the mode shape, which the two element types achieve equally well. Moreover the plate buckling analyses implies, from a mesh resolution view, that the use of continuum shell elements is preferred to conventional shell elements. However, comparing the run times between the conventional and continuum shell element solutions for flat plate buckling presented in Table 3, shows that the run times are equal. Indeed, both run times are equal and low, and thus for these analyses there is little benefit to one element choice over another.

The constant-thickness cylinder frequency analyses presented in Fig. 7b, show behaviors similar to those discussed prior for the constant-thickness plate frequency and buckling analyses. The use of continuum shell elements allows for coarser meshes to be used yet, again, the run time does not show significant benefit. For these coarse mesh resolutions, 30×30 elements, the use of continuum shell elements better approximates the curvature of the cylinder, however there is no run time benefit due to the quick solution computation, which is equal between element types.

For modeling buckling of the constant-angle, constant-thickness cylinder, Fig. 7d, the continuum shell elements begin with similar magnitudes of error to that in the flat plate buckling, Fig. 7c. The primary difference in the response between plate and cylinder buckling is in the rates of convergence. The rate of convergence of the plate is greater than that of the cylinder, where the plate converges upon the 1% criterion at lower mesh resolutions than the cylinder. The cylinder buckling meshes achieve 1% convergence at 100×100 and 110×110 elements for the conventional and continuum shell elements, respectively. Hence, across both structures it is apparent that greater mesh resolution is required for convergence when investigating structural buckling. Moreover, the rate of convergence for both plate and cylinder vibration is greater than that exhibited under buckling.

B. Variable Thickness Structural Discretization By Shell Elements

The effects of increasing mesh resolution on accuracy of resulting linear frequency and buckling eigenvalues for a flat plate and thin-walled cylinder are presented in Fig. 8. For each structure type, two CTS stacking layup designs of increasing discretization difficulty are investigated, where Layup 1 and Layup 2 refer to $[\pm 0\langle 0|70\rangle^{10}]_{2s}$ and $[\pm 0\langle 0|70\rangle^{10}/\pm 90\langle 0|70\rangle^{10}]_{s}$ respectively. For all analyses, the initially investigated element size is based on the recommendation by Meyer-Piening *et al.* for cylinder buckling: $0.5\sqrt{Rt}$, where R is cylinder radius and t is wall thickness [22]. However, this element size recommendation is for use in isotropic cylinders, hence for the highly anisotropic stiffness variations of CTS cylinders it is a useful first-order approximation of mesh density only, not for exact heedance. If this recommendation were followed, it would produce a mesh of such inadequacy that it would not lie within the x-axis range of the presented plots in Fig. 8a. Hence, this motivated the need for iterative refinement of the meshes until sufficient convergence within 1% is achieved.

As presented in Fig. 8a, the conventional shell elements appear to outperform the continuum shell elements for both considered CTS layups for the plate frequency analysis. The conventional shell element model meets the 1% convergence two iteration earlier than the continuum shell element model. The difference in run time does not scale linearly with mesh resolution, hence accuracy is to be sought where possible. This run time nonlinearity is also present in the analysis of constant-angle, constant-thickness structures presented in Section. V.A. The CTS plate frequency analysis indicates that conventional shell elements should be employed in this particular analysis case where convergence is achieved sooner. Earlier convergence allows for coarser meshes and hence comparatively shorter run times per model and thus a more computationally efficient FE modeling tool. In the case of free vibration of CTS plates, the element choice appears to follow that presented prior in Section V.A. For the case of plate free vibration, conventional elements are in fact the superior choice. Moreover, the free vibration of both CTS cylinders also shows similar response to that

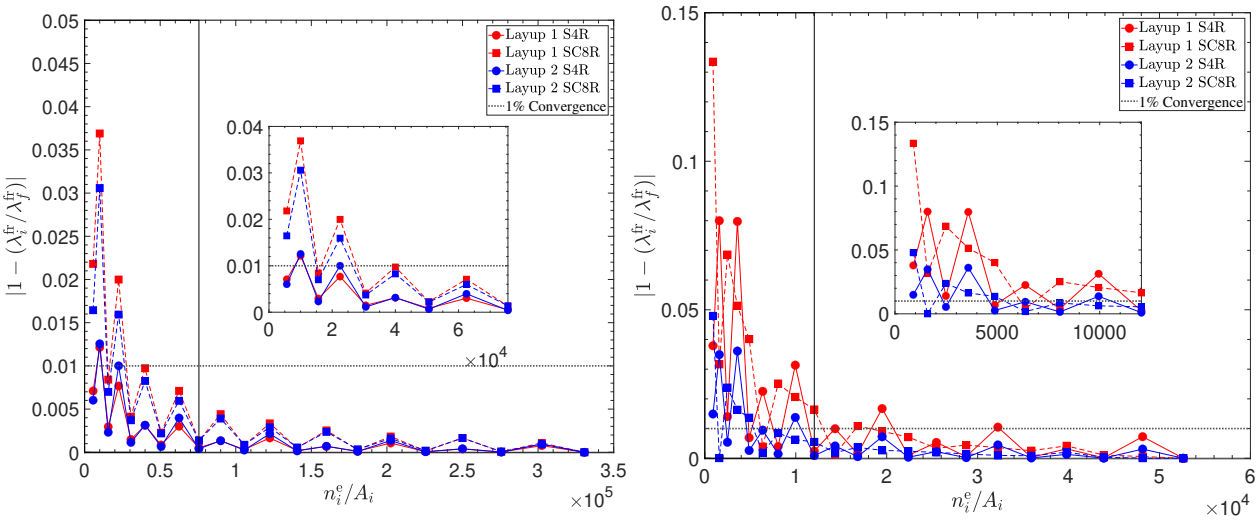

(a) Variable Thickness Plate Frequency

(b) Variable Thickness Cylinder Frequency

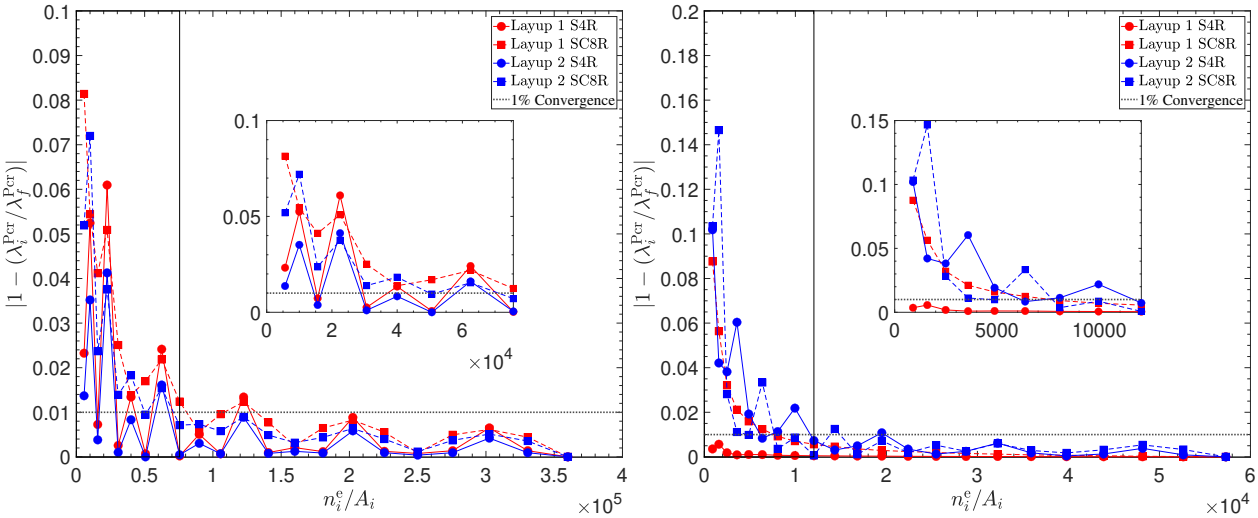

(c) Variable Thickness Plate Buckling

(d) Variable Thickness Cylinder Buckling

Fig. 8 Variable thickness structure eigenvalue approximation of frequency and buckling eigenvalues for each considered structure (flat plate and thin-walled cylinder). Mesh resolutions required for 1% convergence of resulting linear frequency and buckling eigenvalues are are presented in Table 3. Note regions of maximum convergence behavior, i.e. results at low mesh resolutions, are highlighted on each figure as to better identify superior element choices.

Table 4 Meshes required for 1% convergence for variable-thickness structures. N.B. run time refers to solver CPU time and converged mesh refers to a mesh of n^2 elements.

Structure	Analysis	Layup	Element	Converged Mesh	Run Time (s)
Plate	Frequency	1	S4R	75	4
			SC8R	125	12
		2	S4R	75	5
			SC8R	125	12
Plate	Buckling	1	S4R	125	27
			SC8R	300	23
		2	S4R	125	25
			SC8R	225	10
Cylinder	Frequency	1	S4R	175	18
			SC8R	200	33
		2	S4R	125	11
			SC8R	100	9
Cylinder	Buckling	1	S4R	75	26
			SC8R	225	617
		2	S4R	200	233
			SC8R	175	196

in Section V.A, where the rates of convergence are similar between element types, but the continuum shell elements begin with greater accuracy than the conventional shell elements. Thus, there is little benefit to the greater thickness discretization permissible by continuum shell elements.

The benefits of using continuum over conventional shell elements for extracting the critical buckling load of the CTS plates is evident in Fig. 8c, albeit for run time only. This counter-intuitive response is similar also to that discussed prior in Section. V.A, where a finer mesh resolution does not necessarily imply a greater run time. For example, the iteration which achieves the 1% convergence for variable angle, variable thickness plate buckling, for both Layup 1 and 2 require a finer continuum shell element mesh. However, this finer mesh has a lower run time than that found in the conventional shell element solutions. This is particularly evident where the conventional shell element model allows for a 40% coarser mesh, but this comes with a 2.5 times increase in run time. Thus, in general a fine mesh does not necessarily render a greater run time, this is contradictory to what one would presume.

Considering Fig. 8b it is evident that the use of continuum shell elements is of better argument when inspecting Table 4. The continuum shell elements, for Layup 2 ($[\pm 0\langle 0|70\rangle^{10}/\pm 90\langle 0|70\rangle^{10}]_s$) achieve 1% convergence with lower run times than for conventional shell elements. In the case of Layup 2, the mesh resolution required and run time is below that found in the variable angle, variable thickness flat plate frequency and buckling models. The run time benefits of continuum shell elements for layup 2 thin-walled cylinder frequency analysis is 18%. Moreover, when comparing Layups 1 and 2 directly for thin-walled cylinder frequency analysis it is clear that Layup 1 represents a more computationally expensive solution to obtain. Moreover, the notation of Layup 2, $[\pm 0\langle 0|70\rangle^{10}/\pm 90\langle 0|70\rangle^{10}]_s$, denotes a grid-like thickness build-up pattern. This resulting pattern gives equal stiffness variations in both directions on the plate and cylinder. Comparatively Layup 1, $[\pm 0\langle 0|70\rangle^{10}]_{2s}$, denotes transverse or hoop-like thickness build-ups. Hence, Layup 1 has greater stiffness in one direction, this is the transverse and circumferential directions for the plate and cylinder respectively. A stiffness inequality is evidently harder to capture, hence the difference between Layup 1 and 2 eigenvalue results. Furthermore, there is greater potential for mode changes in Layup 1 for increasing mesh density, where the resulting frequency eigenvalues converge slower than those for Layup 2 due to the stiffness asymmetry present in Layup 1.

In the buckling of CTS cylinders, the continuum shell element shows benefit for Layup 2, which is identical to that seen in the frequency analysis of CTS cylinders. For Layup 1, the conventional shell element model converges at rather coarse mesh resolutions (75×75). For Layup 2, the continuum shell demonstrates promising results where a coarser mesh is used to achieve the 1% convergence criterion and as such attains a 15% faster run time. The mixed steering

angles of Layup 2, ($\phi_1 \neq \phi_3$), which cause the grid-like thickness build-ups can be better discretized by continuum shell elements and hence a lower mesh resolution and run time are achieved.

Upon inspection of Fig. 8, one can observe that the convergence behavior of the variable thickness structures does not behave as classically expected, i.e. a smooth exponential decay, such as that seen prior in Fig. 7 for the constant-thickness structures. Instead a non-classical convergence behavior arises due to nuances within the FE discretization algorithm. This non-classical behavior manifests as oscillations to the decay function. These oscillations are present for all variable thickness structures in this manuscript and is not a feature of a single data set only, but of the discretization methodology. However, note that the magnitude of these oscillations decrease as mesh resolution increases. This decrease in oscillations as mesh resolutions increase is due to the relative location of a discretized constant-angle 'slice' to the true analytical thickness variation.

Essentially, the continuum shell elements can capture the minima of the global thickness profile of the CTS structure as the first and last minima corresponds to $x = 0$ and $x = L$, respectively, for $\phi = 0°$. However, as the orientation-thickness coupling is highly non-linear it is pertinent to capture the maxima of the global thickness variation, as both Layup 1 and 2 are highly periodic this is not always assured. The continuum shell element nodes will capture the maxima at select meshes, not all. Moreover, due to the thicknesses of conventional shell elements being assigned by their centroid location, these elements asymptotically approach the maxima of the thickness variation. Thus, as there is inherent variation in the thickness discretization whereby maxima and minima are under and over approximated this has a direct influence upon the stiffness of the discretized structure. As both linear buckling and frequency eigenvalues are driven by stiffness, an under approximation of the maximum thickness results in a under approximation of the maximum stiffness. Hence, as the buckling eigenvalues are proportional to stiffness this results in a lower resulting buckling load, and as such, a premature drop in the accuracy of a mesh iteration. This also holds true for the frequency eigenvalues.

This oscillatory phenomena is presented visually in Fig. 9, for a low periodicity layup ($[\pm 0\langle 0|70\rangle^1]_{2s}$) on the flat plate as a test case. The maximum element thickness, found by conventional shell element centroid locations approaches the continuum shell element maximum nodal thickness, which is a perfect discretization of the true variable thickness geometry in Fig. 9a. Comparatively, Fig. 9b shows a switch between the conventional and continuum shell element discretizations, where the continuum shell elements now asymptotically approach the conventional shell element models. Thus, if an element centroid, in the case of conventional shell elements, does not lie upon a line of maximum thickness then the minimum and maximum thicknesses of the mesh are over and under discretized, respectively. Effectively, an inadequacy arises to the approximation of the global thickness minima and maxima. An ideal mesh allows for the (x, y) - coordinates of the continuum shell element nodes to reside on these lines of maximum thickness. Such an ideal mesh is formulated with an even number of elements in the case of continuum shell elements. As a basic example, consider a single $T_0 \rightarrow T_1 \rightarrow T_0$ shearing period. An even number of elements will allow for the continuum shell element nodes to capture both starting, T_0, and ending, T_1, angles of the period by locating nodes coincident with the thickness minima and maxima. Furthermore, the conventional shell elements, asymptotically converge to the continuum shell discretization, due to the centroids being out-of-phase with the thickness minima and maxima by a half element. However, if the number of elements in the mesh is odd, the $T_0 \rightarrow T_1 \rightarrow T_0$ period is under approximated by the continuum shell elements as the nodes are misaligned with the thickness minima and maxima of the period. In this case, the conventional elements capture the maxima in the thickness profile accurately as the centroid of the conventional shell element is coincident with these points. However, note it is only the maxima that is captured perfectly, there still exists a half element misalignment to the conventional shell elements due to the centroid being inherently located at the center of an element. Hence, meshes presented in Fig. 8 comprising of an odd number of elements represent solutions which under approximate the maximum stiffness of the discretized structure and as such render a lower resulting frequency of buckling eigenvalue from the analyses. This misalignment of nodes and thickness maxima is visualized in Figs. 10 and 11 for even and odd total element counts, respectively.

Hence, there exists three potential solutions to remedy this modeling phenomena. As the oscillations decrease with increasing mesh resolution the phenomena can be mitigated by those meshes which exceed 1% convergence, i.e. at fine mesh resolutions. This, however, is a computationally inefficient solution. To improve modeling efficiencies, if modeling with conventional shell elements meshes with an odd total element count are recommended. Likewise, if modeling with continuum shell elements meshes with an even total element count are recommended to achieve earlier convergence by exploiting element geometries.

Overall, it is clear that all analyses of CTS structures are of increased discretization difficulty in comparison to the constant-thickness analyses presented in Section V.A. In general, the conventional shell element results in quicker convergence and faster run times for Layup 1, where steering and thickness build ups occur in one direction only. For Layup 2, on the other hand, the continuum shell generally lead to faster convergence and quicker run times. This is

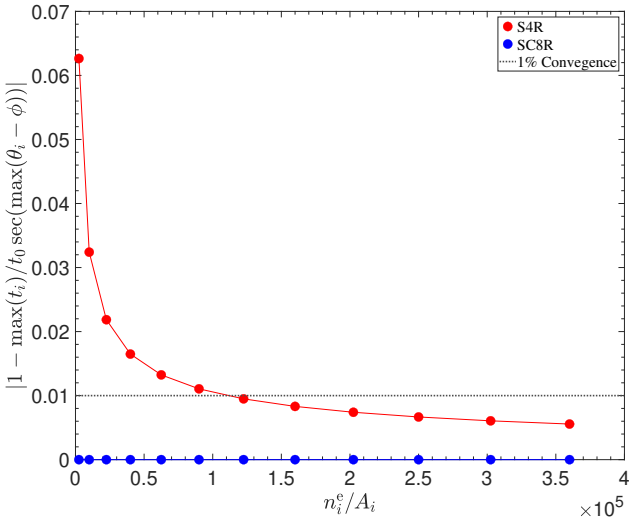

(a) Even total number of elements in mesh

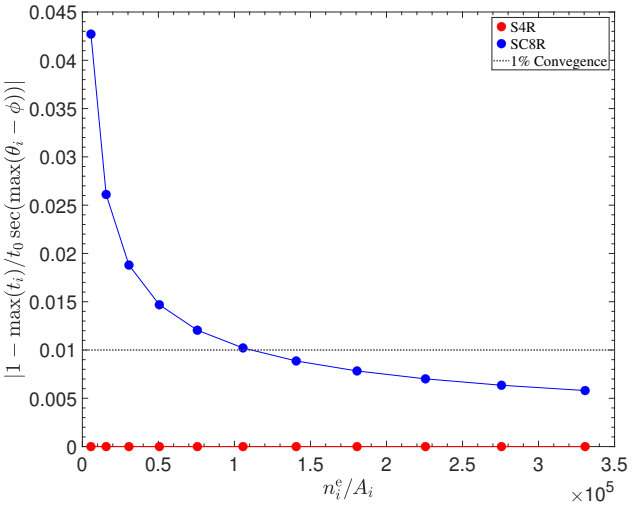

(b) Odd total number of elements in mesh

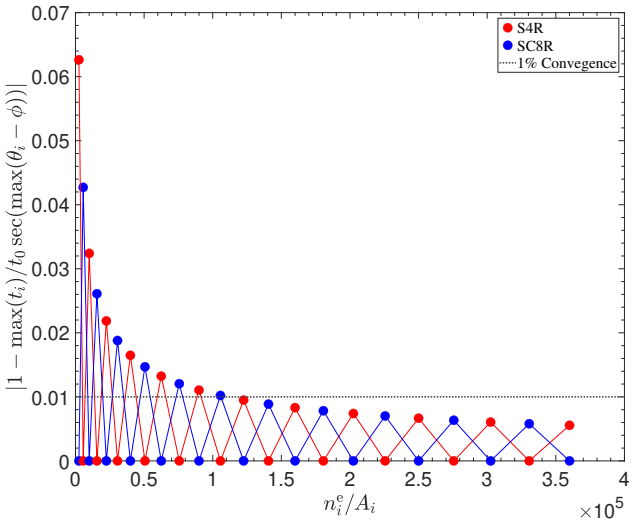

(c) Mixed odd and even numbers of elements in mesh

Fig. 9 Maximum thickness discretization of i^{th} mesh iteration of conventional (S4R) and continuum (SC8R) shell element models for a low periodicity, $[\pm 0\langle 0|70\rangle^1]_{2s}$, CTS plate of dimensions $L = W = 1$ m. The oscillatory convergence of (c) is due to the number of elements varying between odd and even counts. If the mesh consists of an even number of elements, such as that presented in (a), the continuum shell elements can perfectly capture the true thickness variation of the CTS structure, comparatively the conventional shell asymptotically approach the continuum shell element discretization. (b) presents odd total element counts in a mesh. This odd number of elements allows the conventional shell elements to capture the true thickness variations, as evident by the switching of the traces between (a) and (b). Hence, the oscillatory convergence of (c) occurs due to misalignment of periodicity lines with constant-angle 'slices' at odd element counts in the case of the continuum and even in the case of the conventional shell elements.

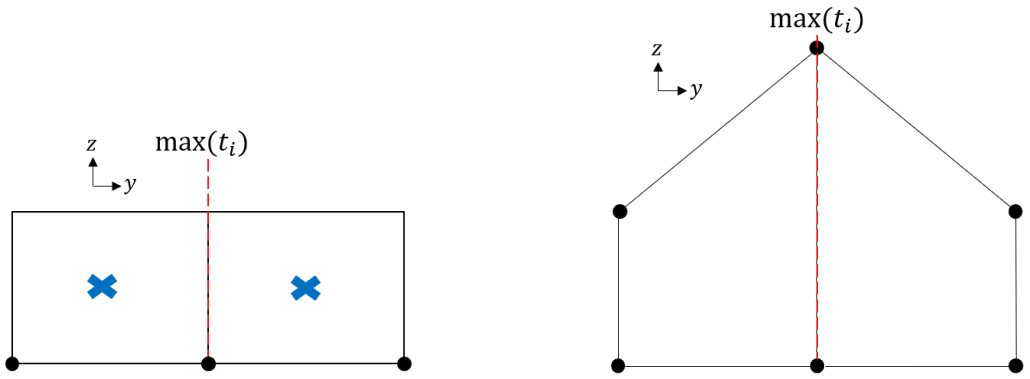

(a) Even conventional element count (b) Even continuum element count

Fig. 10 Even element counts for a demonstratory shearing period in the $z - y$ plane for $\phi = 90$, where the conventional shell elements in (a) cannot capture the maximum of the thickness distribution, $max(t_i)$, as the angles and thus thicknesses are computed at the element centroids, identified by blue crosses). Comparatively, the continuum shell elements in (b) align the nodes with the region of maximum thickness.

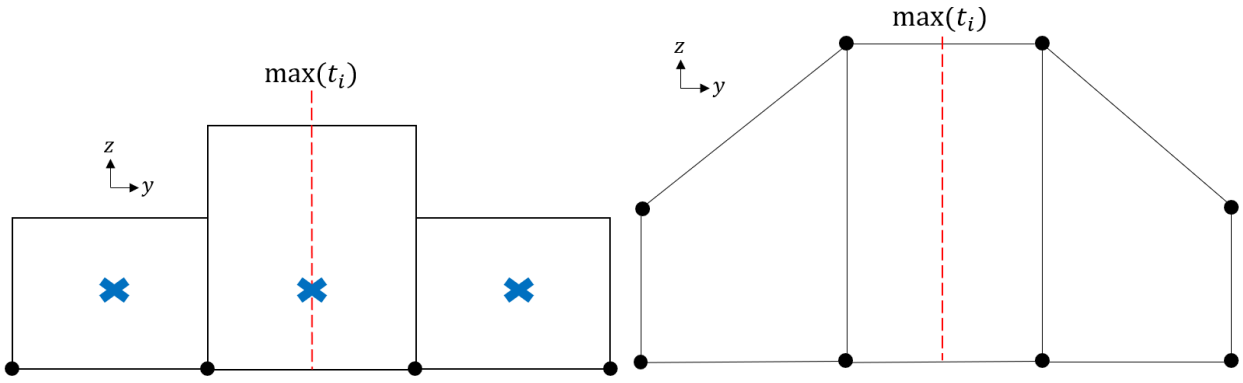

(a) Odd conventional element count (b) Odd continuum element count

Fig. 11 Odd element counts for an demonstratory shearing period in the $z - y$ plane for $\phi = 90$, where the conventional shell elements in (a) can capture the maximum of the thickness distribution, $max(t_i)$, as the angles and thus thicknesses are computed at the element centroids, identified by blue crosses, which are aligned with the region of maximum thickness. Comparatively, the continuum shell elements in (b) cannot capture the region of maximum thickness due to being out-of-phase by half an element.

likely due to the fact that Layup 2 has a more complicated layup with some plies being steered axially and others transversely/circumferentially. This steering scheme creates a highly non-uniform grid-like thickness distribution that is more difficult to model using a single reference plane per element (conventional shell element) than a discretization of the top and bottom surfaces of the laminate (continuum shell element). As such intricate designs with grid-like thickness variation can readily occur in comprehensive optimization studies for various load cases, use of the continuum shell element is generally recommended to give an accurate representation of the asymmetric thickness build-ups of CTS structures. Moreover, one must carefully consider the repercussions of chosen element type on the discretization ability of an employed method. It is critical that, in the case of conventional shell element usage, that the element centroids lie upon a line of maximum thickness. Comparatively, the nodes of a continuum shell element must be coincident with the maxima of the resulting thickness variations when steering by CTS.

VI. Conclusion

This manuscript has investigated the need for modeling with continuum over conventional shell elements for both CTS plates and cylinders with two laminate layups of increasing discretization difficulty. These two structures were chosen due to the increase in surface between a flat plate and thin-walled cylinder. The analysis type selected was both fundamental frequency approximation and critical buckling load determination of the two structures under classical boundary conditions for two different element types. Modeling with both 4-node conventional and 8-node continuum shell elements was undertaken to investigate the hypothesis of increased discretization of the inherent variable thickness geometry of CTS structure due to the non-linear orientation-thickness coupling. In summation, there exist computational benefits for using additional representation of the thickness variations present when analyzing CTS tow-steered structures in certain procedures. Continuum shell elements show increased computational efficiency for plate buckling and cylinder frequency where lower computational cost is required to solve the linear eigenvalue problems. Hence, it is recommended that any convergence analysis undertaken in a modeling investigation be between multiple element types as there may exist benefits of additional node definition in an FE model. The primary benefit of continuum shell element usage is in the superior discretization of the periodic variable thickness of CTS structures. Overall, the potential benefit of superior thickness capture diminishes as mesh resolution increases, the conventional and continuum shell element models converge to an equal result. However, in general accuracy versus run time is the most common consideration to be made in FE modeling when selecting element types. Run time is especially a consideration when conducting design studies, parametric variation or heuristic optimization methods. Thus, the run time savings of continuum elements present the potential for more rapid design iterations in a computational framework. Future work will extend the work to include consideration of imperfections in the analyses where imperfections can interfere with the resulting mode shapes. Hence, if continuum shell elements can give reliably accurate solutions and arrive at consistent mode shapes regardless of imperfections this will further strengthen their use. Moreover, it is expected that further computational efficiencies can be found if meshes are locally refined around the thickness peaks. The non-linearity of the fiber orientation-thickness coupling implies a critical region around the the thickness peaks where a locally refined mesh could be implemented whilst maintaining coarse meshes in-between. Furthermore, adaptive meshing can be expected to provide a highly optimized mesh for a given CTS layup and structural geometry and hence give a model that finds the miniminum run time with coarsest mesh. This optimum mesh produced by adaptive meshing is expected to be the most computationally efficient mesh possible.

Acknowledgments

This work was supported by the Engineering and Physical Sciences Research Council through the EPSRC Centre for Doctoral Training in Composites Science, Engineering and Manufacturing [grant number EP/S021728/1]. R.M.J. Groh acknowledges the support of the Royal Academy of Engineering under the Research Fellowship scheme [Grant No. RF\201718\17178]. This work was carried out using the computational facilities of the Advanced Computing Research Center, University of Bristol - http://www.bris.ac.uk/acrc/. The underlying data for this publication are available through the University of Bristol data repository.

References

[1] Reddy, J., *Mechanics of Laminated Composite Plates and Shells: Theory and Analysis*, 2nd ed., CRC Press, Boca Raton, 2004.

[2] Xin, Z., Duan, Y., Xu, W., Zhang, T., and Wang, B., "Review of the mechanical performance of variable stiffness design

fiber-reinforced composites," *IEEE Journal of Selected Topics in Quantum Electronics*, Vol. 25, No. 3, 2018, pp. 425–437. https://doi.org/10.1515/secm-2016-0093.

[3] Hyer, M. W., and Charette, R. F., "Use of curvilinear fiber format in composite structure design," *AIAA Journal*, Vol. 29, No. 6, 1991, pp. 1011–1015. https://doi.org/10.2514/3.10697.

[4] Wu, K. C., "Design and analysis of tow-steered composite shells using fiber placement," *American Society for Composites - 23rd Technical Conference of the American Society for Composites 2008*, Vol. 2, No. September 2008, 2008, pp. 1124–1141.

[5] Qu, W., He, R., Cheng, L., Yang, D., Gao, J., Wang, H., Yang, Q., and Ke, Y., "Placement suitability analysis of automated fiber placement on curved surfaces considering the influence of prepreg tow, roller and AFP machine," *Composite Structures*, Vol. 262, No. January, 2021, p. 113608. https://doi.org/10.1016/j.compstruct.2021.113608, URL https://doi.org/10.1016/j.compstruct.2021.113608.

[6] Heinecke, F., and Willberg, C., "Manufacturing-Induced Imperfections in Composite Parts Manufactured via Automated Fiber Placement," *Journal of Composites Science*, Vol. 3, No. 2, 2019, p. 56. https://doi.org/10.3390/jcs3020056.

[7] Kim, B. C., Potter, K., and Weaver, P. M., "Continuous tow shearing for manufacturing variable angle tow composites," *Composites Part A: Applied Science and Manufacturing*, Vol. 43, No. 8, 2012, pp. 1347–1356. https://doi.org/10.1016/j.compositesa.2012.02.024.

[8] Li, X., Hallett, S. R., and Wisnom, M. R., "Modelling the effect of gaps and overlaps in automated fibre placement (AFP)-manufactured laminates," *Science and Engineering of Composite Materials*, Vol. 22, No. 2, 2015, pp. 115–129. https://doi.org/10.1515/secm-2013-0322.

[9] Fayazbakhsh, K., Arian Nik, M., Pasini, D., and Lessard, L., "Defect layer method to capture effect of gaps and overlaps in variable stiffness laminates made by Automated Fiber Placement," *Composite Structures*, Vol. 97, 2013, pp. 245–251. https://doi.org/10.1016/j.compstruct.2012.10.031, URL http://dx.doi.org/10.1016/j.compstruct.2012.10.031.

[10] Labans, E., and Bisagni, C., "Buckling and free vibration study of variable and constant-stiffness cylindrical shells," *Composite Structures*, Vol. 210, No. August 2018, 2019, pp. 446–457. https://doi.org/10.1016/j.compstruct.2018.11.061.

[11] Rouhi, M., Ghayoor, H., Hoa, S. V., and Hojjati, M., "Multi-step design optimization of variable stiffness composite cylinders made by fiber steering," *Proceedings of the American Society for Composites - 29th Technical Conference, ASC 2014; 16th US-Japan Conference on Composite Materials; ASTM-D30 Meeting*, , No. June 2016, 2014.

[12] Dassault Systèmes Simulia Corp., *Abaqus Theory Manual*, 6th ed., Dassault Systèmes Simulia Corp., Providence, 2014.

[13] Tatting, B. F., "Design and Manufacture Tow Placed Plates of Elastically Tailored," , No. August, 2020.

[14] Kim, B. C., Weaver, P. M., and Potter, K., "Manufacturing characteristics of the continuous tow shearing method for manufacturing of variable angle tow composites," *Composites Part A: Applied Science and Manufacturing*, Vol. 61, 2014, pp. 141–151. https://doi.org/10.1016/j.compositesa.2014.02.019.

[15] Lincoln, R. L., Weaver, P. M., Pirrera, A., and Groh, R. M., "Imperfection-insensitive continuous tow-sheared cylinders," *Composite Structures*, Vol. 260, 2021, p. 113445. https://doi.org/10.1016/j.compstruct.2020.113445, URL https://doi.org/10.1016/j.compstruct.2020.113445.

[16] Lincoln, R. L., Weaver, P. M., Pirrera, A., and Groh, R. M., "Optimization of imperfection-insensitive continuous tow sheared rocket launch structures," *AIAA Scitech 2021 Forum*, , No. January, 2021, pp. 1–19. https://doi.org/10.2514/6.2021-0202.

[17] Kim, B. C., Weaver, P. M., and Potter, K., "Computer aided modelling of variable angle tow composites manufactured by continuous tow shearing," *Composite Structures*, Vol. 129, 2015, pp. 256–267. https://doi.org/10.1016/j.compstruct.2015.04.012, URL http://dx.doi.org/10.1016/j.compstruct.2015.04.012.

[18] Groh, R. M., and Weaver, P. M., "Mass optimization of variable angle tow, variable thickness panels with static failure and buckling constraints," *56th AIAA/ASCE/AHS/ASC Structures, Structural Dynamics, and Materials Conference*, , No. January, 2015, pp. 5–9.

[19] White, S. C., Weaver, P. M., and Wu, K. C., "Post-buckling analyses of variable-stiffness composite cylinders in axial compression," *Composite Structures*, Vol. 123, 2015, pp. 190–203. https://doi.org/10.1016/j.compstruct.2014.12.013, URL http://dx.doi.org/10.1016/j.compstruct.2014.12.013.

[20] Gürdal, Z., and Olmedo, R., "In-plane response of laminates with spatially varying fiber orientations: Variable stiffness concept," *AIAA Journal*, Vol. 31, No. 4, 1993, pp. 751–758. https://doi.org/10.2514/3.11613.

[21] MathWorks, "MATLAB (Version 2021b)," , 2021.

[22] Meyer-Piening, H. R., Farshad, M., Geier, B., and Zimmermann, R., "Buckling loads of CFRP composite cylinders under combined axial and torsion loading - experiments and computations," *Composite Structures*, Vol. 53, No. 4, 2001, pp. 427–435. https://doi.org/10.1016/S0263-8223(01)00053-8.